Nanoscale

Designing 1D Multiheme Peptide Amphiphile Assemblies Reminiscent of Natural Systems

Journal:	*Nanoscale*
Manuscript ID	NR-ART-01-2022-000473.R1
Article Type:	Paper
Date Submitted by the Author:	11-May-2022
Complete List of Authors:	Fry, Harry; Argonne National Laboratory, Center for Nanoscale Materials Divan, Ralu; Argonne National Laboratory, Center for Nanoscale Materials Liu, Yuzi; Argonne national Laboratory, Center for Nanoscale Materials

ARTICLE

Designing 1D Multiheme Peptide Amphiphile Assemblies Reminiscent of Natural Systems

H. Christopher Fry,* Ralu Divan, and Yuzi Liu

Received 00th January 20xx,
Accepted 00th January 20xx

DOI: 10.1039/x0xx00000x

Protein assemblies that bind and organize ordered arrays of cofactors yield functiona structures. Multiheme assemblies found in nature yield electronically conductivity 1D nanoscale fibers and are employed in anaerobic respiration. To understand the fundamental characteristics of these organized arrays, the design of peptide amphiphiles that assemble into 1D nanostructures and yield metalloporphyrin binding sites is presented. One challenge with this class of peptide amphiphiles is identifying the correct sequence composition for high affinity binding with high heme density. Here, the peptide c16-AH(Kx)n –CO_2H is explored to identify the impact of sequence length (n) and amino acid identity (x = L, I, or F) on binding affinity and midpoint potential. When n = 2, the peptide assembly yields the greatest affinity. The resulting nanoscale assemblies yield ordered arrays of the redox active molecule heme and have potential utility in the development of supramolecular bioelectronic materials useful in sensing as well as the development of enzymatic materials.

Introduction

Multi-heme proteins possess the ability to shuttle electrons across long distances, Figure 1A&C.[1-2] This is achieved via proteins assembling the chromophore in long aspect ratio, well-ordered arrays. It is apparent that the interplay between protein architecture, amino acid content, heme coordination and heme ordering play important roles in yielding efficient charge hopping pathways over long distances, Figure 1B&D. Some bacterial protein filaments are conductive and have potential utility as bioelectronic media.[3-4] Therefore, the development of a highly modular, synthetic analog capable of forming 1D nanostructures would facilitate the understanding of the natural system and provide a platform for developing novel materials.

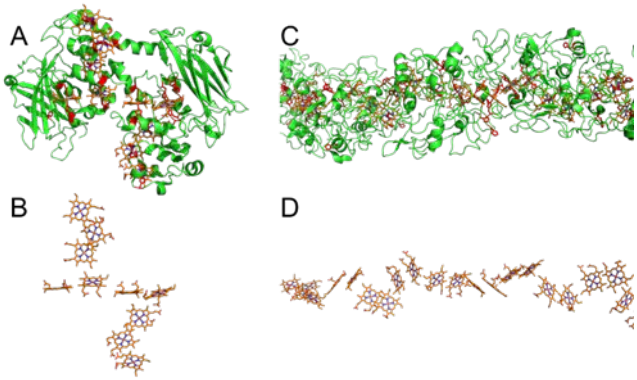

Figure 1. Cartoon rendering of the MtrC protein (PDB ID – 6QYC) (A) and the resulting heme organization (B) from *Shewanella oneidensis*. Cartoon rendering of the OmcS protein (PDB ID – 6EF8) (C) and the resulting heme organization (D) from *Geobacter sulfurreducens*.

Significant efforts have been reported trying to understand the interplay between coherent and incoherent long range electron transport[5] as well as the contributing factors such as precisely placed redox active, aromatic amino acids (Tyrosine and Tryptophan) that facilitate the electron transport mechanism.[3, 6-7] van Wonderen and co-workers have performed thorough analysis on the heme-heme electron transfer and long range electron transport mechanism by modifying the MTRc protein with a $Ru(bpy)_3$ moiety and have identified that the mechanism, i.e. the rate of charge separation, can be tuned by modifying the active site from a His-His to a His-Met coordination environment.[8-9] Vargas and co-workers removed all aromatic amino acids and replaced them with alanine which led to a loss of electronic conductivity.[6] Other electronically conductive peptide/protein wires have been explored simply by organizing aromatic amino acids (no cofactor) in either α–helix[10] or β-sheet[11] rich supramolecular assemblies suggesting that either secondary structural morphology can facilitate electronic conductivity. Supramolecular peptide assemblies represent an excellent class of materials capable of addressing many of these variables.

Through rational design of peptide amphiphiles, 1D nanoscale architectures[12] can be achieved and heme molecules are coordinated to an engineered bis-histidine coordination environment.[13-15] The simplicity of the design (alkyl tail-binding site-aliphatic β-sheet-charged head group) makes it possible to

Address: *Center for Nanoscale Materials, Argonne National Laboratory, 9700 S. Cass Avenue, Lemont, IL 60439*

Electronic Supplementary Information (ESI) available: [details of any supplementary information available should be included here]. See DOI: 10.1039/x0xx00000x

explore the sequence space of the peptide in an effort to determine how sequence impacts various properties of the heme molecule. Previous examples have explored varying the coordination environment, the aliphatic beta sheet sequence, the patterning of the sequence, and the length of the alkyl tail.[13-15] Each of these "tuning knobs" affects the supramolecular organization of the peptide assembly as well as the local coordination and micro- environment surrounding the heme molecule yielding different binding affinities and stoichiometry. Previously, the materials were assembled at high pH values (~11) to effectively neutralize the charged lysine head group, reducing the electrostatic repulsion between neighboring molecules, thus initiating the assembly of long aspect ratio, β-sheet rich peptide fibers. Recently, the peptide c16-AH(KL)$_3$-CONH$_2$ was determined to assemble at pH > 7, just above the pKa of histidine.[13] Essentially, the histidine, when charged, precludes assembly in this particular sequence. Here, the peptides c16-AH(Kx)$_n$ (where n = 1 – 4 and x = L, I, or F and denoted simply as PA-KL1, PA-KL2, etc.), Figure 2, are explored to examine how the length of the peptide sequence and the identity of the hydrophobic amino acid (i.e. aliphatic vs. aromatic) impacts the heme binding affinity, heme density, and the electronic properties.

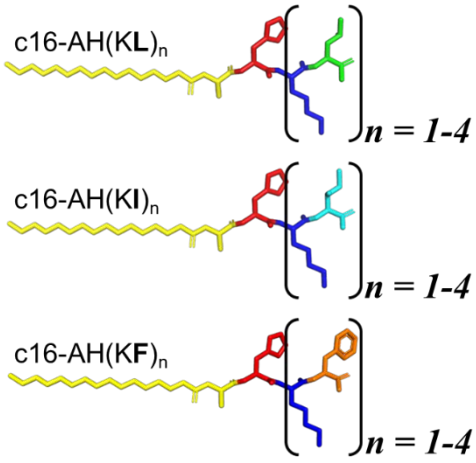

Figure 2. Peptides investigated in this study c16-AH(KL)$_n$, c16-AH(KI)$_n$, and c16-AH(KF)$_n$ where n = 1-4. Color code: c16 modified alanine, yellow; histidine, red; lysine, blue; leucine, green; isoleucine, cyan; phenylalanine, orange

Results and Discussion

The peptide series PA-Kx*n* demonstrates increasing hydrophobicity with decreasing (Kx) repeat units as indicated by the increasing retention time in the RP-HPLC chromatograms (Figure S1). Peptides were prepared as stock solutions in water at a concentration of 10 mg/mL and diluted as needed. All peptides except PA-KL1 demonstrated the ability to assemble into β-sheet rich structures at pH 8 (Tris buffer) as measured by circular dichroism spectroscopy[16] (minima at 218 nm) and maintain their β-sheet character as dried films as indicated by

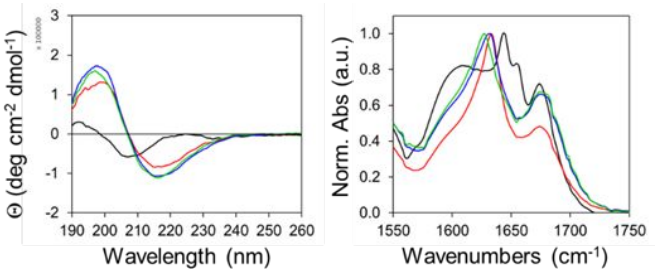

Figure 3. Secondary structure characterization of PA-KL*n* in A) Tris buffer, pH 8 using CD spectroscopy and B) dried films from Tris buffer solutions using Fourier transform infrared (FTIR) spectroscopies. Color coding: Black, PA-KL1; Red, PA-KL2; Blue, PA-KL3; and Green, PA-KL4. Analogous data for PA-KIn and PA-KFn can be found in Figure S2.

infrared spectroscopy[17] (Amide 1 vibrations at 1627 and 1673 cm^{-1}), Figure 3 and S2. [Note: prior to this work, most results were reported in water and the pH was adjusted with ammonium hydroxide to induce self-assembly. The identification of histidine as the pH trigger[13] influenced the decision to work in Tris buffer at pH 8.] In investigations of similar peptides, the kinetics of β-sheet formation were notably slower.[13, 18] But β-sheet formation here occurred during the preparation of the sample in Tris buffer. The percentage of β-sheet content was determined by fitting the CD data using BetStSel.[16] The resulting secondary structure distribution data suggest substantial β-sheet content but not as dominant as expected, Table S1. However, self-assembled peptides with long range ordering often lead to unusual CD spectra due to their extended electronic networks making quantification of secondary structure challenging with the fitting algorithms.[19-20] As a result, we observe unusually high percentages of α-helices which we consider to be highly unlikely in these short peptides and are in disagreement with the FTIR data that demonstrate amide I vibrations consistent with a dominant β-sheet composition. PA-KL1 demonstrated an unusual circular dichroism (CD) spectrum with minima at 208 and 235 nm and the infrared spectrum yielded amide I vibrations (1606(br), 1643, 1656, and 1673 cm^{-1}). The results from secondary structural analysis are consistent with the spectral observations in FTIR (i.e. α-helix = 1656 cm^{-1}). suggest that the peptide assembly is comprised of 31% α-helices, 20% β-sheet, and 49% random coil.

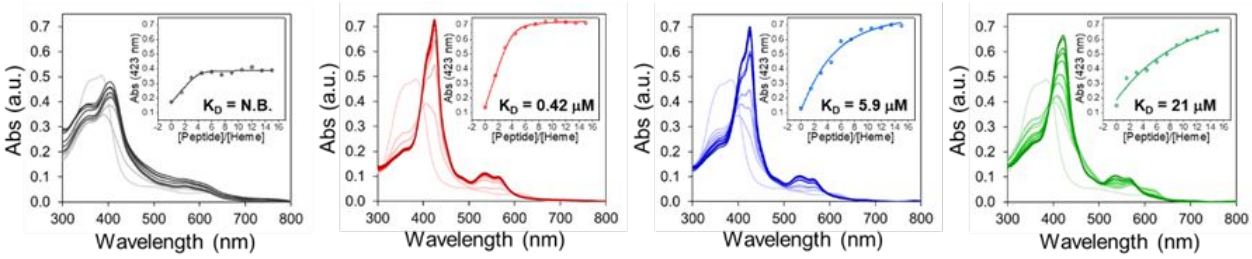

Figure 4. Binding constant analysis of PA-KL*n* (0 – 150 μM) into heme (10 μM) in Tris buffer, pH 8 monitored by UV/visible spectroscopy. Color coding: Black, PA-KL1; Red, PA-KL2; Blue, PA-KL3; and Green, PA-KL4. Analogous data for PA-KIn and PA-KFn can be found in Figure S3.

The binding affinity (K_D) of heme to the pre-assembled peptides was investigated, Figure 4, Figure S3 and Table 1. Individual samples were prepared by introducing various concentrations of pre-assembled peptides to a heme solution (10 μM in Tris buffer) and aged for 24 hrs. In general, heme in buffer yields a spectrum with Soret = 398 nm and Q-band = 505 and 625 nm consistent with hemin (PPIX)Fe^{III}(Cl). Upon addition of 1 eq of peptide, we observe an immediate transition to Soret = 400 nm and Q-band = 570, 610 nm. This suggests that there is a preliminary interaction with the peptide assembly prior to histidine coordination. Upon increasing the peptide concentration further, signal intensity and Soret-splitting is observed in most cases. PA-KL1 does not bind heme via histidine coordination as indicated by the lack of spectral change typical of histidine coordination. However, the introduction of the peptide to the heme solution indicates a slight change in the spectra intensity that we propose is the encapsulation of heme in the supramolecular peptide assembly that lacks a suitable environment for facilitating bis-His heme coordination. A similar spectrum was obtained in an earlier investigation where all histidines were removed from the peptide c16-$A_2L_3K_3$-CO_2H (Soret, 401 nm; Q-band, 567, 610 nm).[15] The greatest affinity for heme was observed with PA-KL2 where coordination via bis-histidine axial ligation is indicated by the growth of a split Soret at 409 and 426 nm and Q-band feature at 532, 560 nm, Figure 4. This result was replicated by introducing heme into a solution of PA-KL2 at a fixed concentration to verify that the split Soret was not due to a mixture of free and bound heme, Figure S4. Typically, bis-histidine ligated heme exhibits a Soret maximum at 412-414 nm. The UV/vis spectra of PA-KL2 are similar to that observed from earlier studies where at pH 11 PA-KL3 exhibited a similar split Soret at 409 and 426 nm indicative of exciton coupling between neighboring chromophores.[14] The splitting is demonstrably less pronounced with increasing peptide length as seen in the titration data for PA-KL3 and PA-KL4. While exciton coupling is observed in the natural systems highlighted in Figure 1, Soret splitting is not observed and the peak positions in the natural system are blue shifted due to the c-type nature of the heme.[21-22] The electronic absorption spectrum generated by our synthetic system is unusual. However, there exists one example in the literature of a multiheme protein that exhibits a split Soret spectrum, the aptly named split-Soret cytochrome C.[23] The ferric state of the protein does not exhibit the split Soret (λ_{max} = 408 nm), but the ferrous state does with λ_{max} = 424 and 415 nm as opposed to other ferrous multiheme proteins that exhibit a single, sharp Soret band centered at 418.5 nm. The crystal structure highlights two heme-heme dimer entities, with similar heme-heme geometries to other multiheme proteins, i.e. edge-edge distance of ~4 Å.[24]

Analysis of the heme affinity from the titration data using eq. 1 affords two important parameters, the stoichiometry (*n*) and the dissociation constant (K_D). A strong correlation with the length of the repeat unit in the PA-KL*n* series was observed spanning nearly two orders of magnitude (0.42 to 21 μM) and indicated that four peptide molecules were required to bind a single heme molecule, Figure 4. This stoichiometry of 4:1 is different than measurements reported prior to this study where stoichiometries ranging from 6:1 to 10:1 were observed in different solvent conditions (100 mM ammonium hydroxide, pH 11) than the buffer used in this study. A similar trend in heme affinity is observed for the PA-KI*n* series where the highest affinity was observed for PA-KI2. Interestingly, PA-KI1 was observed to bind heme albeit with markedly lower affinity than PA-KI2. PA-KF to PA-KF4 does not yield a split-Soret. Instead, a

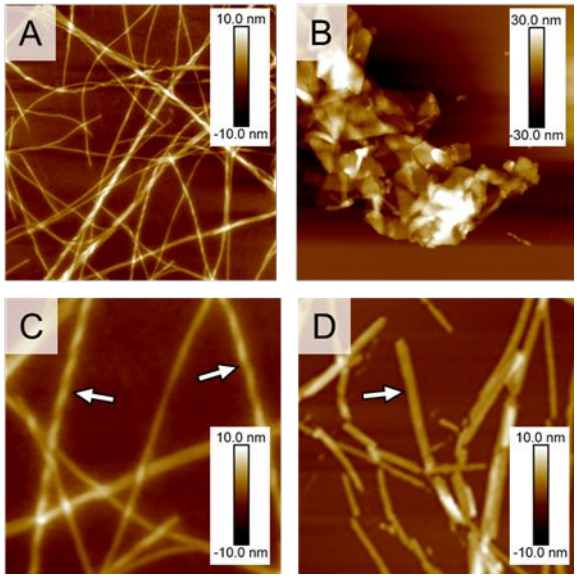

Figure 5. Atomic force micrographs of PA-KL2 (A) highlighting typical β-sheet rich nanofibers, PA-KL1 (B) exhibiting large sheet-like assemblies devoid of b-sheets, PA-KL-2 close-up highlighting the super-helical structure (C) and PA-KF2 image detailing "flat" or "belt-like" fibers (D). Scale: A and B are 2 x 2 μm micrographs while C and D are 1 x 1 μm.

"textbook" example of a bis-histidine coordinated heme molecule with Soret, 412 nm and q-band, 532, 560 nm is observed and is consistent with a similar class of β-sheet rich/heme binding peptides from the group of S. Bhattacharjya.[25] All of the binding affinities measured for PA-KF2 to PA-KF4 were within experimental error (K_D = 1.3 to 2.9 μM) whereas PA-KF1 did not bind heme but similarly to PA-KL1 encapsulated the heme molecule, Figure S3.

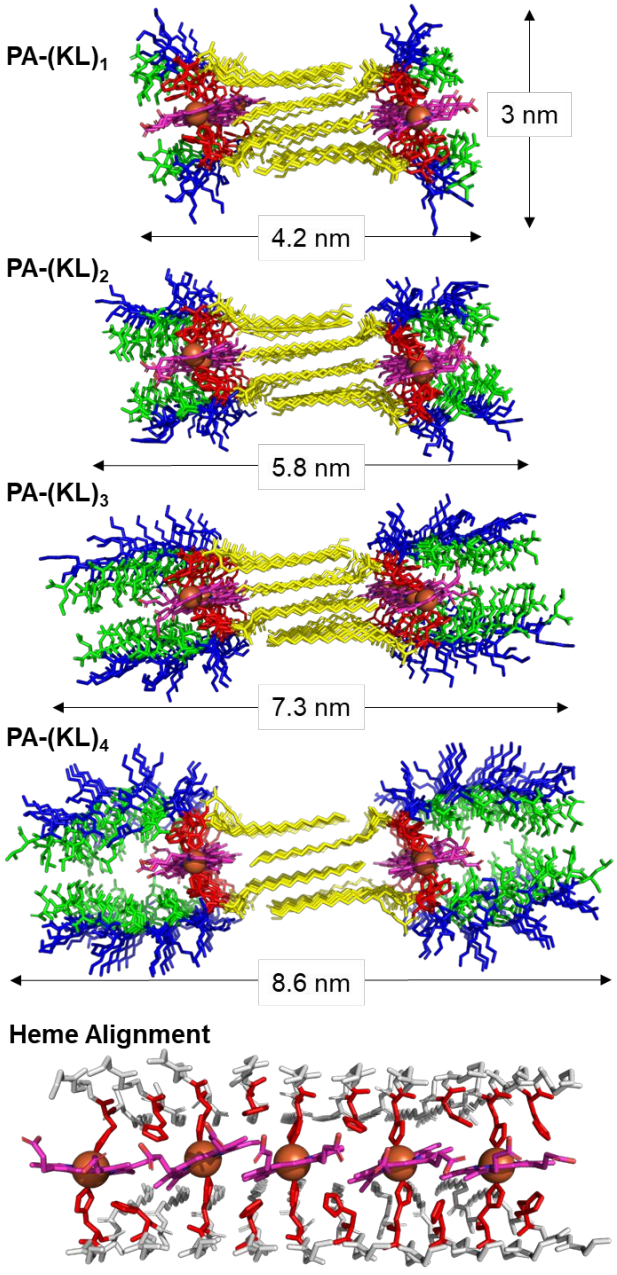

Circular dichroism was employed to further explore the possibility of heme-heme exciton coupling, Figure S5. In PA-KL2 to PA-KL4 an intense negative spectrum is observed and is indicative of the impact of the supramolecular environment on the heme coordination environment.[22, 26] There is literature precedence that suggests CD spectra of metalloporphyrin proteins that lack a bisignate shape are indicative of exciton coupling between amino acid side chains and the heme molecule.[27] In fact, heme/histidine coupling is likely as many of the histidine molecules within the assembly are not coordinated to heme (Figure 6). However, the split-Soret feature observed in the UV/visible spectra suggests exciton coupling exists between neighboring chromophores and may contribute to the CD signal as well. Furthermore, the CD spectra for the PA-KI*n* and PA-KF*n* series are noticeably less intense and suggests that the aliphatic leucine residue yields a unique microenvironment that promotes the highest degree of chiroptic activity.

Figure 6. Energy minimized renderings of PA-KL1, PA-KL2, PA-KL3, and PA-KL4 highlighting the molecular packing around the heme molecules. The progression from PA-KL2 to PA-KL4 clearly highlights poor van der Waals packing between the hydrophobic leucine residues (green) and the heme molecule (magenta) as the repeat length increases. Bottom: The resulting heme overlap with an average edge to edge distance of 4.3 Å as a result of the 4:1 stoichiometry in a β-sheet rich assembly.

The morphology of the assemblies were characterized with atomic force microscopy. All peptides, with the exception of PA-KL1, yield long aspect ratio nanofibers regardless of repeat unit length and sequence, Figure 5 and S6-S8. PA-KL1 yielded nanoscale sheets, Figure 5B. Individual sheets exhibited heights of ~ 13 nm, Figure S7A. The difference in morphology between PA-KL1 and all other assemblies reported here can be correlated with the difference in secondary structure lacking extended β-sheets as characterized by both FT-IR and CD spectroscopies. Height analysis for individual nanofibers were performed for each peptide, Figure S7, and summarized in table S2. All heights measured are within experimental error of one another, 3.9 ± 0.4 nm, suggesting that the height measured most likely is not due to the length of the peptide as one would observe a systematic increase in the fiber size as *n* increases, e.g. n = 1 yields 4.2 nm, n= 4 yields 8.6 nm, Figure 6 and Table S3. We propose that the height measured is in fact due to the proposed stacked assembly where the average measured height is ~ 3 nm and is independent of repeat unit (*n*), Figure 6. Among the 1D nanofiber assemblies, the only difference noted was the presence of superhelical or twisted structures in the PA-KL*n* series and the lack thereof in PA-KF*n*. The superhelical assembly for PA-KL2 yields varying heights of 5 nm and 8 nm, Figure S8. The lack of a superhelical structure in the PA-KF*n* series is attributed to potential aromatic packing between neighboring phenyl groups.[28-29] This observation is noticeable in the structures observed by cryogenic transmission electron microscopy (cryoTEM) PA-KL3 that indicates a mixture of belts and fibers while PA-KF3 indicates a strong preference towards extended belts (possibly 2D sheets), Figure S9. These morphologies are consistent with other PA assemblies that follow the pattern alkly tail-pnpn (where p = polar amino acid and n = non-polar amino acid) and yielded giant nanobelts.[30] Finally, it should be noted that all micrographs indicate a tendency of the fibers to aggregate into larger bundled structures as a means of packing the hydrophobic core and is a well observed phenomenon in peptide self-assembly.[31]

The peptide assemblies were modeled based on our characterization results. The CD spectra in the far-UV and the IR spectra indicated predominantly β-sheet rich assemblies in 50 mM Tris, 100 mM NaCl, pH 8.0. The AFM, indicate long aspect ratio nanofibers in all cases with a few examples indicating superhelical structures. Therefore, in our molecular model, we

pre-assemble 10 peptides in a parallel β-sheet array that yields a hydrophobic face rich in either leucine, isoleucine, or phenylalanine. Two of the decamer assemblies are then "sandwiched" together and the palmitoyl tails are interdigitated with a second decamer sandwich for further modeling, e.g. structure optimization via energy minimization of the holo assemblies, Figure 6 and Figure S10. The UV/vis suggest bis-histidine coordination and in conjunction with the 4:1 stoichiometry, 5 heme molecules are added to the decameric "sandwich" assembly, Figure 6 (bottom). The total assembly consists of 40 peptides and 10 heme molecules.

In order to assess the molecular structures and the resulting heme binding site, the distance between the aliphatic residues opposite one another in the "sandwich" structure were measured and summarized in Table S4. In the structures of PA-KL1 and PA-KF1, we find that the heme molecule is coordinated but partially exposed to water, Figure S11, resulting in an unfavorable binding site. When we increase the length of the (Kx) repeat unit to PA-KL2 and PA-KF2, the heme molecule becomes buried in the hydrophobic pocket. Our initial supposition was that the more buried the hydrophobic pocket, the greater the binding affinity. However, as the repeat unit increases from *n* = 2 to 4, the peptide assembly appears to bow, Figure S12. This is monitored by measuring the increasing average distance between leucine residues from opposite assemblies, Leu6-Leu6', Table S4. This directly impacts the heme binding site in which van der Waals interactions become less favorable as *n* increases and is reflected in the distance measured between Leu4 and the meso-carbon of the heme molecule, Figure S13 and Table S4. We find that PA-KL2 yields the closest moleculsr interactions with Leu4-meso carbon = 3.7 ± 0.2 Å and Leu6-Leu6' = 4.4 ± 0.4 Å. As a result, PA-KL2 yields the most favorable binding site and is consistent with our experimental work where PA-KL2 exhibits the highest binding affinity. This is in contrast to PA-KL4 where Leu6-Leu6' = 10.1 ± 3.2 Å and Leu4-meso carbon = 5.3 ± 1.7 Å suggesting a less suitable heme binding environment due to unfavorable molecular packing. Upon changing the assignment of the aliphatic leucine residue to phenylalanine, we observe one major difference. The Phe4-meso carbon distance is less impacted by the increasing peptide length, *n* = 2 to 4, than in the case of leucine, Table S4. The average Phe4 to meso carbon distance is 4.9 ± 0.3 Å. As a result, the phenylalanine rich assembly is consistent from *n* = 2 to 4 yielding a similar heme binding pocket regardless of repeat length. This is consistent with our experimental results in which the binding constant (K_D) was not significantly impacted by the length of the repeat unit, Table 1.

Most interestingly in the modeling study, we find that the 4:1 stoichiometry leads to overlapping heme molecules with an average edge to edge distance of 4.3 Å close to that found in conductive multi-heme proteins (Edge to edge = 4.2 Å for MtrA in *S. oneidensis* and 3.6 Å for OmcS in *G. sulfurreducens*) .[1-2] The biggest difference in the edge to edge measurements is that the natural systems exhibit pairs of heme (edge to edge ~ 4 Å) that are separated by a ~ 6 Å gap. This natural phenomenon replicated in two different organisms most likely suggests a significant structural component to yielding conductive nanowires. Due to the non-covalent nature of introducing heme to the PA-Kx*n* series, it is possible to control the average distance between neighboring chromophores simply by adjusting the number of heme molecules added per unit of peptide.

Peptide	Binding Constant (μM)	Midpoint Potential (mV vs Ag/AgCl)
PA-KL*1*	x	-328
PA-KL*2*	0.42	-379
PA-KL*3*	5.9	-360
PA-KL*4*	21	-328
PA-KI*1*	12	-355
PA-KI*2*	1	-377
PA-KI*3*	4.5	-377
PA-KI*4*	12	-377
PA-KF*1*	x	-338
PA-KF*2*	1.3	-361
PA-KF*3*	2.9	-357
PA-KF*4*	2.4	-362

Table 1. Summary of binding constants and midpoint potentials. x – histidine coordination not observed. Heme midpoint potential = -390 mV vs. Ag/AgCl (See Figure Sx)

We are interested in these assemblies to access their electronic properties to develop conductive nanofibers to mimic the natural cytochrome assemblies in *S. oneidensis* and *G. sulfurreducens*. Here, we employ thin film voltammetry in an effort to observe the impact of the microenvironment and binding affinity on the midpoint potential of the heme molecules. The midpoint potential is only moderately sensitive to the peptide coordination environment, Figure S14 and Table 1. Heme in the absence of peptide yields a -390 mV vs. Ag/AgCl redox potential, Figure S15. Heme proteins have a wide range of midpoint potentials depending on their coordination mode and local microenvironment. They are most influence in the case of c-type cytochromes where a nucleophilic substitution between a cysteine and vinyl group yields a heme molecule covalently attached to the protein yielding a thioether bond.[32] The difference between the redox potential of a system that is coordinatively attached to the peptide assembly (e.g. PA-KL2) vs. simply encapsulated heme with no histidine coordination (e.g. PA-KL1) indicates a slight change. When the peptide binds the chromophore via bis-histidine axial ligation with high affinity, we observe a lower redox potential at ~ -370 ± 10 mV vs. Ag/AgCl compared to the samples with the lowest (or unobserved) binding affinity (~ 330 ± 10 mV vs Ag/AgCl). This observation suggests that a high affinity binding site yields a lower redox potential. Due to the exciton splitting of the Soret band, we expected a more dramatic change in the redox potential.

Due to the similarity in nanoscale assembly to the naturally occurring systems, conductivity measurements in the presence and absence of heme in two of the assemblies PA-KL2 and PA-

KF2 were measured. First, the absorption spectrum of a film of the dried PA-KL2: Heme (4:1) assembly on glass was measured to verify that the heme molecules remained coordinated to the assembly, Figure S16. The AFM image of the material dropcast onto the interdigitated electrodes indicates that a network of fibers spanned across the gaps of the interdigitated electrodes, Figure S17. The IV plots (Figure S18) indicate a substantial Schottky barrier in the PA-KL2:Heme and PA-KF2:Heme assemblies. In the absence of heme, the Schottky barrier is still present but is less intense. It must be noted that reproducing the data proved challenging (Figure S18C) suggesting that the random orientation of the fibers with respect to the interdigitated electrodes is difficult to control. Our results suggest that our peptide/heme fibers potentially possess the ability to conduct electrons but must be manipulated to align thus ensuring a more direct and uniform path of electron transfer spanning the intraband gap.

Our evidence from spectroscopy, binding affinity, redox behavior, and morphological analysis are highly reminiscent of the naturally occurring, conductive nanoscale assemblies for *G. sulfurreducens* and *S. oneidensis*. At a 4:1 peptide:heme stoichiometry, the findings presented here represent the most dense heme concentration within a peptide amphiphile assembly. However, we have yet to achieve a structure that performs efficiently as an electronically conductive nanofiber in a manner similar to the natural systems. Therefore, we refer back to the natural system to identify the main differences with our synthetic assembly. First, our peptide assembly employs non-covalently bound heme in a bis-Histidine coordination motif (typically classified as a heme B protein) whereas the conductive protein nanowires are not only bis-Histidine coordinated but also covalently attached to cysteine residues to the vinyl groups of the heme cofactor yielding c-type heme coordination. C-type cytochromes typically have a higher redox potential and could contribute to the efficient long range electron transport properties observed in the natural systems.[1-2, 32] Secondly, the heme array may need to be electronically coupled to the peptide via engineered interactions with tyrosine or tryptophan, for example, to facilitate electron/hole mobility. Gray and Winkler have reported on the importance of hole conduction in cytochromes.[3, 7, 33] Proton coupled electron transfer may be critical to the efficiency of conductive heme protein fibers. Finally, many of the measurements made on the conductivity of the heme rich proteins were made of highly aligned fibers. There is significant evidence that this mechanical manipulation will lead to better material performance. Supramolecular peptide assemblies offer the versatility to not only manipulate the peptide sequence for control over the immediate coordination environment as described here, but also the ability to manipulate the structure into highly aligned bundled arrays.[34] Tovar and co-workers have highlighted the importance of aligning fibers comprised of a bola-amphiphilic peptide terthiophene conjugate in order to achieve quantifiable conductivity.[35] Fortunately, employing synthetic self-assembling peptides facilitates the ability to explore all of these variations in future iterations of this class of multi-heme binding assemblies.

Conclusions

We have demonstrated how to improve binding affinity (K_D) with high heme packing density (4:1 peptide:heme ratio) when designing multiheme supramolecular peptide assemblies. By exploring the generic peptide sequence c16-AH$(Kx)_n$ where x = Leu, Ile, Phe and n = 1-4, we found that decreasing the repeat number from 4 to 2 yields an improved binding affinity when x = Leu or Ile (in Tris buffer at pH 8). Interestingly, when x = Phe we did not observe a dramatic change in heme binding affinity suggesting that phenylalanine provides a similar binding environment for heme when n = 2 - 4. However, when n = 1 and x = Leu, Ile, or Phe, we observed a significant loss in the binding affinity if not a complete lack of histidine coordination to heme attributed to the insufficient van der Waals contact stemming from the short peptide. The identification of these various design parameters, like repeat length and amino acid packing, is critical for identifying new materials that self-assemble and bind various energy relevant cofactors that are found in nature. Our future investigations plan on unlocking nature's ability to yield electronically conductive nanoscale fibers through sequence and structure variations of the peptide assembly.

Materials and Methods

Peptide Synthesis and Purification Solid-phase peptide synthesis (SPPS) of c16-AH$(Kx)_n$-$CONH_2$ was carried out using standard Fmoc chemistry (CS Bio Co. automated peptide synthesizer, CS136XT). Rink amide MBHA resin, low load (0.25mmol synthetic scale, loading capacity: 0.39 mmol/g, Chem Impex) was used as the solid support. A solution of 20% piperidine (Sigma-Aldrich) in dimethylformamide (Fisher Chemical, Bioreagent Grade) was used as the deprotecting reagent with subsequent 5 and 20 minute deprotection times. Coupling was executed using four fold equivalents of standard Fmoc protected amino acids (1 mmol, Chem Impex) and stoichiometric equivalents of diisopropylethylamine (DIEA, 1 mmol, Sigma Aldrich) and O-Benzotriazole-N,N,N',N'-tetramethyl-uronium-hexafluoro-phosphate (HBTU, 1mmol, Chem Impex) in DMF with a 90 minute coupling time. Fmoc-His(trt)-OH (1mmol, Chem Impex) was double coupled, with successive 90 minute coupling times. Palmitic acid (c16, Chem Impex) was quadruple coupled (subsequent 90 minute coupling reactions) to the N-terminus of the peptide using DIEA (1 mmol) and HBTU (1 mmol). Note: HBTU functionalized alkyl chains are relatively insoluble in DMF and require additional rinsing steps with dichloromethane. Finally, the resin was rinsed with dicholoromethane and dried via nitrogen purge for 1 hr.

Upon completion of the synthesis, the peptide side chains were deprotected and the crude peptide removed from the peptidyl resin with a standard trifluoroacetic acid solution (10 mL, 95% TFA, 2.5% triisopropylsilane, 2.5% water) in a fritted peptide reaction vessel for 3 h (Chemglass Inc.). The resulting solution

was filtered into a 20 mL glass vial. The crude peptide was precipitated out of solution via dropwise addition of the TFA solution into cold diethyl ether (90 mL). The suspension in diethyl ether was transferred into two centrifuge tubes. The precipitate was pelleted using a centrifuge. The off-white to white precipitate was washed thrice with cold-diethyl ether yielding the crude material.

All peptides were purified using an Agilent Technolgies HPLC Workstation (Agilent 1260 Infinity) equipped with a c18 column (Jupiter Proteo 10x250 mm, Phenomenex). A modified linear purification method was employed using a polar mobile phase water (0.1% TFA) with a 1% (v/v) per minute increase of the non-polar mobile phase acetonitrile (0.1% TFA). The sample was prepared at a concentration of 10 mg/mL in water (0.1% TFA) with injection volumes of 0.9 mL. The sample eluted between 50 and 60% acetonitrile (0.1% TFA). The purified peptide was isolated by removing acetonitrile via rotary evaporation followed by freeze drying to yield the pure peptide material as a white powder. Advion Expression CMS (ESI-MS) was employed to determine the correct mass of the isolated peptides. Peptide purity >95% was verified using a linear gradient method using the same setup described for semi-preparative purification.

Stock Solutions: Each peptide (3-4 mg) was dissolved in nanopure water (Millipore A10) to obtain a 1 wt% solution. Hemin (Sigma-Aldrich) was dissolved in DMSO (Sigma Aldrich) to achieve a 10 mM stock solution. Note: Hemin/DMSO stock solutions were made to ensure that the final DMSO concentration in the sample was less than 1% (v/v).

Secondary Structure: Circular dichroism (JASCO J-815, Jasco Inc.) and fourier transform infrared spectroscopies (Thermofisher Nicolet) were employed to determine the secondary structure of the peptide assemblies. Peptide samples for CD spectroscopy were prepared by adding a small volume of the 1 wt% stock solutions into Tris buffer (50 mM, 150 mM NaCl, pH 8) for a final peptide concentration of 150 μM. The solution was transferred to a 1 mm quartz cuvette. An average of three spectra were recorded from 190 – 260 nm. Infrared spectra were obtained by dropcasting 10 μL of a 1.5 mM peptide solution (in Tris Buffer) onto a CaF_2 window and drying the sample. The spectra represent an average of 16 scans with 4 cm^{-1} resolution from 1500 -1800 cm^{-1}.

Heme binding. Heme titration experiments were performed as follows. Heme (10 mM) in 1 mL of Tris buffer was added to 11 disposable plastic cuvettes (10 mm pathlength). Increasing quantities of peptide were added to each cuvette from 0 in the first cuvette to 150 μM in the eleventh (i.e. 15 μM aliquots between cuvettes). The samples were covered with parafilm and aged in the dark at room temperature for 24 hrs. The samples were monitored by UV/visible spectroscopy (Cary 60 UV/visible spectrometer, Agilent Technologies) by scanning from 300 - 800 nm with a 1 nm resolution. Equation 1 was employed for stoichiometry and binding constant analysis is modified from a 1:1 binding model. The value 'n' is introduced here and represents the stoichiometry of peptide to heme. Ao, initial absorption; ϵ_B, extinction of bound heme; ϵ_s, extinction coefficient contribution from scattering; x, ratio of peptide to heme; n, stoichiometry of peptide to heme; K_d, dissociation (binding) constant; M, molar concentration of heme; l, cuvette pathlength. Origin was used for data analysis.

$$A = Ao + \frac{\epsilon_B l}{2} \times \left(\left(\frac{x}{n} \times M + K_D + M\right) - \sqrt{\left(\frac{x}{n} \times M + K_D + M\right)^2 - 4 \times \frac{x}{n} \times M^2}\right) - \epsilon_S \times l \times M + \frac{\epsilon_S l}{2} \times \left(\left(\frac{x}{n} \times M + K_D + M\right) - \sqrt{\left(\frac{x}{n} \times M + K_D + M\right)^2 - 4 \times \frac{x}{n} \times M^2}\right)$$

Eq. 1.

Circular dichroism (JASCO J-815, Jasco Inc.) in the visible region was employed to observe the exciton coupling between neighboring chromophores. Samples were prepared at 1.5 mM Peptide and 100 μM Heme in Tris buffer. The samples were transferred to 1 mm cuvette. An average of three spectra were recorded from 350 - 500 nm.

Morphology: Atomic force microscopy was obtained on a Bruker MultiMode 8 microscope using the Scanasyst mode. A silicon tip on a nitride lever was used (Scanasyst-Air Probe, Bruker). Samples were prepared via drop casting 100 μL of a 150 μM peptide solution (diluted in water from a 1.5 mM Peptide in Tris buffer solution) on freshly cleaved mica. After 30 seconds the solution was removed via pipet followed by wicking away the remaining solution with filter paper. 2 μm x 2 μm images were collected at a scan rate of 1 Hz.

Sample vitrification for cryoTEM was performed using a Mark IV Vitrobot (ThermoFisher Scientific) Plunge Freezing system for TEM grid preparation. Samples were prepared at 500 ?M concentration. 3 μL of the solution was deposited on an ultrathin carbon film on a lacey carbon support, 400 mesh, copper grid (Ted Pella). The sample was imaged by using Fischione Cryo Transfer Tomography Holder on an FEI-Tecnai F20 operated at 200kV.

Thin film voltammetry: Electrochemistry measurements were made with a BASI Electrochemical Workstation. Samples (10 μL of a 1.5 mM peptide:100 μM heme solution) were dropcast and dried on a freshly polished glassy carbon working electrode. A platinum wire served as the auxiliary electrode while a Ag/AgCl reference electrode was used. The potential was swept from -0.1 to -0.6 V at various scan rates. The measurements were made in 50 mM Tris buffer, 100 mM NaCl, at pH 8.0. Blank voltammograms, i.e. unfunctionalized glassy carbon electrode in Tris buffer, were subtracted from the data at corresponding scan rates. All numbers reported in the text are vs. Ag/AgCl.

Conductivity: Conductivity measurements were performed by depositing a 2 μL droplet of the peptide assembly (PA-KL2 or PA-KF2, 1 mM; or PA-KL2:Heme or PA-KF2:Heme, 1 mM:0.25 mM) onto an interdigitated gold electrode. The electrode was comprised of 100 parallel 5 μm × 2 mm long bands with an intraband spacing of 5 μm. Devices were photolithographically patterned onto glass slides with 60 nm Au and a 5 nm Ti adhesion layer deposited by electron beam evaporation. Atomic force microscopy was used to analyze the fiber organization spanning the intraband spacing of the electrodes. A linear sweep voltage from -2.0 to 2.0 V (0.04 V steps) was measured using a 2 probe method on a Keithley Probe Station.

Modeling: The peptides were pre-assembled (Hyperchem 8.0) into decameric parallel, β-sheet assemblies. Two of the decamers were assembled such that the hydrophobic faces were sandwiched together (20 peptide molecules). Since the spectroscopy indicated a 4:1 peptide:heme stoichiometry, 5 heme molecules were inserted at the bis-histidine binding sites and coordinated to the histidine ε–nitrogen. Two of these resulting assemblies were arranged with the aliphatic tails interdigitated. As a result, 40 peptide molecules and 10 heme molecules were pre-assembled and energy minimized *in vacuo* using CHARMM 27 force field. These modeling studies are primarily used for assembly illustration, but are based entirely off of experimental evidence revealing a 4:1 stoichiometry in a β-sheet rich nanoscale assembly.

Author Contributions

H.C.F. performed the experimental work and wrote the manuscript. R.D. fabricated the interdigitated electrode and edited the manuscript. Y.L. performed CryoTEM and edited the manuscript.

Conflicts of interest

There are no conflicts to declare.

Acknowledgements

Work performed at the Center for Nanoscale Materials, a U.S. Department of Energy Office of Science User Facility, was supported by the U.S. DOE, Office of Basic Energy Sciences, under Contract No. DE-AC02-06CH11357.

Notes and references

1. Wang, F. B.; Gu, Y. Q.; O'Brien, J. P.; Yi, S. M.; Yalcin, S. E.; Srikanth, V.; Shen, C.; Vu, D.; Ing, N. L.; Hochbaum, A. I.; Egelman, E. H.; Malvankar, N. S., Structure of Microbial Nanowires Reveals Stacked Hemes that Transport Electrons over Micrometers. **2019,** *177* (2), 361-369.

2. Edwards, M. J.; White, G. F.; Butt, J. N.; Richardson, D. J.; Clarke, T. A., The Crystal Structure of a Biological Insulated Transmembrane Molecular Wire. **2020,** *181* (3), 665-673.

3. Ing, N. L.; El-Naggar, M. Y.; Hochbaum, A. I., Going the Distance: Long-Range Conductivity in Protein and Peptide Bioelectronic Materials. *J. Phys. Chem. B* **2018,** *122* (46), 10403-10423.

4. Lovley, D. R.; Yao, J., Intrinsically Conductive Microbial Nanowires for 'Green' Electronics with Novel Functions. **2021,** *39* (9), 940-952.

5. Ru, X. Y.; Zhang, P.; Beratan, D. N., Assessing Possible Mechanisms of Micrometer-Scale Electron Transfer in Heme-Free Geobacter sulfurreducens Pili. *J. Phys. Chem. B* **2019,** *123* (24), 5035-5047.

6. Vargas, M.; Malvankar, N. S.; Tremblay, P. L.; Leang, C.; Smith, J. A.; Patel, P.; Synoeyenbos-West, O.; Nevin, K. P.; Lovley, D. R., Aromatic Amino Acids Required for Pili Conductivity and Long-Range Extracellular Electron Transport in Geobacter sulfurreducens. *mBio* **2013,** *4* (2).

7. Gray, H. B.; Winkler, J. R., Hole hopping through tyrosine/tryptophan chains protects proteins from oxidative damage. *Proc. Natl. Acad. Sci. U. S. A.* **2015,** *112* (35), 10920-10925.

8. van Wonderen, J. H.; Hall, C. R.; Jiang, X. Y.; Adamczyk, K.; Carof, A.; Heisler, I.; Piper, S. E. H.; Clarke, T. A.; Watmough, N. J.; Sazanovich, I. V.; Towrie, M.; Meech, S. R.; Blumberger, J.; Butt, J. N., Ultrafast Light-Driven Electron Transfer in a Ru(II)tris(bipyridine)-Labeled Multiheme Cytochrome. *J. Am. Chem. Soc.* **2019,** *141* (38), 15190-15200.

9. van Wonderen, J. H.; Adamczyk, K.; Wu, X. J.; Jiang, X. Y.; Piper, S. E. H.; Hall, C. R.; Edwards, M. J.; Clarke, T. A.; Zhang, H. J.; Jeuken, L. J. C.; Sazanovich, I. V.; Towrie, M.; Blumberger, J.; Meech, S. R.; Butt, J. N., Nanosecond heme-to-heme electron transfer rates in a multiheme cytochrome nanowire reported by a spectrally unique His/Met-ligated heme. *Proc. Natl. Acad. Sci. U. S. A.* **2021,** *118* (39).

10. Hochbaum, A.; Ing, N.; Spencer, R., Electronic transport in supromolecular peptide nanofibers. *Abstr. Pap. Am. Chem. Soc.* **2018,** *255*.

11. Shipps, C.; Kelly, H. R.; Dahl, P. J.; Yi, S. M.; Vu, D.; Boyer, D.; Glynn, C.; Sawaya, M. R.; Eisenberg, D.; Batista, V. S.; Malvankar, N. S., Intrinsic electronic conductivity of individual atomically resolved amyloid crystals reveals micrometer-long hole hopping via tyrosines. *Proc. Natl. Acad. Sci. U. S. A.* **2021,** *118* (2).

12. Wei, G.; Su, Z. Q.; Reynolds, N. P.; Arosio, P.; Hamley, I. W.; Gazit, E.; Mezzenga, R., Self-assembling peptide and protein amyloids: from structure to tailored function in nanotechnology. **2017,** *46* (15), 4661-4708.

13. Fry, H. C.; Peters, B. L.; Ferguson, A. L., Pushing and Pulling: A Dual pH Trigger Controlled by Varying the Alkyl Tail Length in Heme Coordinating Peptide Amphiphiles. **2021,** *125* (5), 1317-1330.

14. Fry, H. C.; Wood, A. R.; Solomon, L. A., Supramolecular control of heme binding and electronic states in multi-heme peptide assemblies. **2017,** *15* (32), 6725-6730.

15. Solomon, L. A.; Kronenberg, J. B.; Fry, H. C., Control of Heme Coordination and Catalytic Activity by Conformational Changes in Peptide-Amphiphile Assemblies. **2017,** *139* (25), 8497-8507.

16. Micsonai, A.; Wien, F.; Kernya, L.; Lee, Y. H.; Goto, Y.; Refregiers, M.; Kardos, J., Accurate secondary structure prediction and fold recognition for circular dichroism spectroscopy. **2015,** *112* (24), E3095-E3103.

17. Kong, J.; Yu, S., Fourier transform infrared spectroscopic analysis of protein secondary structures. **2007,** *39* (8), 549-559.

18. Deshmukh, S. A.; Solomon, L. A.; Kamath, G.; Fry, H. C.; Sankaranarayanan, S., Water ordering controls the dynamic equilibrium of micelle-fibre formation in self-assembly of peptide amphiphiles. **2016,** *7*.

19. Manning, M. C.; Illangasekare, M.; Woody, R. W., CIRCULAR-DICHROISM STUDIES OF DISTORTED ALPHA-HELICES, TWISTED BETA-SHEETS, AND BETA-TURNS. *Biophys. Chem.* **1988,** *31* (1-2), 77-86.

20. Zhang, S. G., Discovery of the first self-assembling peptide, study of peptide dynamic behaviors, and G protein-coupled receptors using an Aviv circular dichroism spectropolarimeter. *Biopolymers* **2018,** *109* (8).

21. Tomlinson, E. J.; Ferguson, S. J., Conversion of a c type cytochrome to a b type that spontaneously forms in vitro from apo protein and heme: Implications for c type cytochrome biogenesis and folding. **2000,** *97* (10), 5156-5160.

22. Tokunou, Y.; Chinotaikul, P.; Hattori, S.; Clarke, T. A.; Shi, L.; Hashimoto, K.; Ishii, K.; Okamoto, A., Whole-cell circular dichroism difference spectroscopy reveals an in vivo-specific deca-heme conformation in bacterial surface cytochromes. **2018,** *54* (99), 13933-13936.

23. Liu, M. C.; Costa, C.; Coutinho, I. B.; Moura, J. J. G.; Moura, I.; Xavier, A. V.; Legall, J., CYTOCHROME COMPONENTS OF NITRATE-RESPIRING AND SULFATE-RESPIRING DESULFOVIBRIO-DESULFURICANS ATCC 27774. *J. Bacteriol.* **1988,** *170* (12), 5545-5551.

24. Abreu, I. A.; Lourenco, A. I.; Xavier, A. V.; LeGall, J.; Coelho, A. V.; Matias, P. M.; Pinto, D. M.; Carrondo, M. A.; Teixeira, M.; Saraiva, L. M., A novel iron centre in the split-Soret cytochrome c from Desulfovibrio desulfuricans ATCC 27774. *J. Biol. Inorg. Chem.* **2003,** *8* (3), 360-370.

25. D'Souza, A.; Bhattacharjya, S., De Novo-Designed beta-Sheet Heme Proteins. **2021,** *60* (6), 431-439.

26. Oohora, K.; Fujimaki, N.; Kajihara, R.; Watanabe, H.; Uchihashi, T.; Hayashi, T., Supramolecular Hemoprotein Assembly with a Periodic Structure Showing Heme-Heme Exciton Coupling. **2018,** *140* (32), 10145-10148.

27. Hsu, M. C.; Woody, R. W., ORIGIN OF HEME COTTON EFFECTS IN MYOGLOBIN AND HEMOGLOBIN. *J. Am. Chem. Soc.* **1971,** *93* (14), 3515-+.

28. Gazit, E., A possible role for pi-stacking in the self-assembly of amyloid fibrils. **2002,** *16* (1), 77-83.

29. Wychowaniec, J. K.; Patel, R.; Leach, J.; Mathomes, R.; Chhabria, V.; Patil-Sen, Y.; Hidalgo-Bastida, A.; Forbes, R. T.; Hayes, J. M.; Elsawy, M. A., Aromatic Stacking Facilitated Self-Assembly of Ultrashort Ionic Complementary Peptide Sequence: beta-Sheet Nanofibers with Remarkable Gelation and Interfacial Properties. **2020,** *21* (7), 2670-2680.

30. Cui, H.; Muraoka, T.; Cheetham, A. G.; Stupp, S. I., Self-Assembly of Giant Peptide Nanobelts. **2009,** *9* (3), 945-951.
31. Aggeli, A.; Nyrkova, I. A.; Bell, M.; Harding, R.; Carrick, L.; McLeish, T. C. B.; Semenov, A. N.; Boden, N., Hierarchical self-assembly of chiral rod-like molecules as a model for peptide beta-sheet tapes, ribbons, fibrils, and fibers. *Proc. Natl. Acad. Sci. U. S. A.* **2001,** *98* (21), 11857-11862.
32. Reedy, C. J.; Gibney, B. R., Heme protein assemblies. **2004,** *104* (2), 617-649.
33. Winkler, J. R.; Gray, H. B., Could tyrosine and tryptophan serve multiple roles in biological redox processes? *Philos. Trans. R. Soc. A-Math. Phys. Eng. Sci.* **2015,** *373* (2037).
34. Zhang, S. M.; Greenfield, M. A.; Mata, A.; Palmer, L. C.; Bitton, R.; Mantei, J. R.; Aparicio, C.; de la Cruz, M. O.; Stupp, S. I., A self-assembly pathway to aligned monodomain gels. *Nat. Mater.* **2010,** *9* (7), 594-601.
35. Wall, B. D.; Diegelmann, S. R.; Zhang, S. M.; Dawidczyk, T. J.; Wilson, W. L.; Katz, H. E.; Mao, H. Q.; Tovar, J. D., Aligned Macroscopic Domains of Optoelectronic Nanostructures Prepared via Shear-Flow Assembly of Peptide Hydrogels. *Adv. Mater.* **2011,** *23* (43), 5009-5014.